Monthly Notices of the ROYAL ASTRONOMICAL SOCIETY

MNRAS **499,** 3976–3991 (2020) doi:10.1093/mnras/staa2905
Advance Access publication 2020 September 23

High-amplitude γ Doradus variables

Ernst Paunzen [1], Klaus Bernhard,[2,3] Stefan Hümmerich [2,3]★ Franz-Josef Hambsch,[2,3,4] Christopher Lloyd[5] and Sebastián Otero[3]

[1]*Department of Theoretical Physics and Astrophysics, Masaryk University, Kotlářská 2, CZ-611 37 Brno, Czech Republic*
[2]*Bundesdeutsche Arbeitsgemeinschaft für Veränderliche Sterne e.V. (BAV), Munsterdamm 90, D-12169 Berlin, Germany*
[3]*American Association of Variable Star Observers (AAVSO), 49 Bay State Road, Cambridge, MA 02138, USA*
[4]*Vereniging Voor Sterrenkunde (VVS), Zeeweg 96, B-8000 Brugge, Belgium*
[5]*Department of Physics and Astronomy, University of Sussex, Falmer Campus, Brighton BN1 9QH, UK*

Accepted 2020 September 18. Received 2020 September 18; in original form 2020 April 16

ABSTRACT

According to most literature sources, the amplitude of the pulsational variability observed in γ Doradus stars does not exceed 0.1 mag in Johnson *V*. We have analysed fifteen high-amplitude γ Doradus stars with photometric peak-to-peak amplitudes well beyond this limit, with the aim of unraveling the mechanisms behind the observed high amplitudes and investigating whether these objects are in any way physically distinct from their low-amplitude counterparts. We have calculated astrophysical parameters and investigated the location of the high-amplitude γ Doradus stars and a control sample of fifteen low-amplitude objects in the $\log T_{\rm eff}$ versus $\log L/L_{\odot}$ diagram. Employing survey data and our own observations, we analysed the photometric variability of our target stars using discrete Fourier transform. Correlations between the observed primary frequencies, amplitudes and other parameters like effective temperature and luminosity were investigated. The unusually high amplitudes of the high-amplitude γ Doradus stars can be explained by the superposition of several base frequencies in interaction with their combination and overtone frequencies. Although the maximum amplitude of the primary frequencies does not exceed an amplitude of 0.1 mag, total light variability amplitudes of over 0.3 mag (*V*) can be attained in this way. Low- and high-amplitude γ Doradus stars do not appear to be physically distinct in any other respect than their total variability amplitudes but merely represent two ends of the same, uniform group of variables.

Key words: stars: oscillations – stars: variables: general.

1 INTRODUCTION

The γ Doradus and δ Scuti stars are pulsating variables that are situated in the region of the A and F-type main-sequence stars. For convenience, they are referred to hereafter as, respectively, GDOR and DSCT stars, according to their designations in the General Catalogue of Variable Stars (GCVS; Samus et al. 2009). In contrast to the long-known and very well-studied DSCT stars (Fath 1935; Breger 2000), the variability of GDOR stars was discovered relatively recently. They were identified as a new class of variables by Balona, Krisciunas & Cousins (1994) and defined as such by Kaye et al. (1999).

The GDOR stars are characterized by high-order, low-degree, non-radial gravity (g) mode pulsation (Kaye et al. 1999), which is thought to be driven by the convective flux blocking mechanism (Guzik et al. 2000; Dupret et al. 2005). They are encountered between spectral types A7 and F7 (GCVS), although other sources have shifted the red border of the GDOR instability strip to somewhat hotter temperatures. Balona et al. (2011), for instance, find most GDOR stars in the effective temperature range from $6500 < T_{\rm eff} < 7000$ K, corresponding to spectral types F1 to F5 on the main sequence, while Bradley et al. (2015) find all of their GDOR candidates between $6100 < T_{\rm eff} < 7500$ K. However, it has been shown that there are also hot GDOR stars, which are located between the red edge of the Slowly Pulsating B star and the blue edge of the GDOR star instability strips (Balona et al. 2016; Kahraman Aliçavuş et al. 2020).

GDOR and DSCT stars can be distinguished by the time-scales of the observed variability, although the instability strips for both classes overlap and hybrid-types exist (e.g. Henry & Fekel 2005). Several different classification systems are found in the literature. According to the GCVS, GDOR stars exhibit variability in the period range of $0.3 \leq P \leq 3$ d ($0.33 \leq f \leq 3.33\,{\rm d}^{-1}$) (cf. Kaye et al. 1999), while DSCT stars are encountered in the period range of $0.01 \leq P \leq 0.2$ d ($5 \leq f \leq 100\,{\rm d}^{-1}$). Based on an analysis of high-precision *Kepler* photometry, Grigahcène et al. (2010) proposed a division into 'pure' DSCT stars ($f > 5$ c/d), 'pure' GDOR stars ($f < 5$ c/d), and hybrid types exhibiting variability in both frequency regimes. While hybrid-type pulsators are mostly discovered in ultra-precise space photometry, their frequency of occurrence (∼25 per cent of the sample of Uytterhoeven et al. 2011) has made clear that the situation is complex and the traditional classification scheme might be in need of revision. The understanding and relationship of DSCT and GDOR pulsators is currently in flux (e.g. Grigahcène et al. 2010; Uytterhoeven et al. 2011; Balona et al. 2011; Balona 2012, 2018; Antoci et al. 2019).

★ E-mail: ernham@rz-online.de

Using *Kepler* data, Balona et al. (2011) described three groups of distinct GDOR star light curves. Two of these groups show pronounced beating effects. These are the SYM stars, which show more or less symmetric light curves and the ASYM stars, whose light curves are asymmetric in the sense that the beat amplitude is larger when the star is brighter, which results in large variations in maximum brightness but only small variations in minimum brightness. The third group is made up of the MULT stars, which are characterized by many low-amplitude peaks that do not lead to pronounced beating in the light curve.

Kaye et al. (1999) indicated a photometric peak-to-peak amplitude[1] of up to 0.1 mag in Johnson *V* for GDOR variables. This limit has been widely accepted and is found throughout the literature and variability catalogues, like e.g. the International Variable Star Index of the AAVSO (VSX; Watson 2006). The GCVS somewhat softens this statement, indicating that peak-to-peak amplitudes are *usually* up to 0.1 mag. In fact, at the time of this writing (2020 March), only 24 out of the 924 GDOR variables contained in the VSX are listed with amplitudes exceeding 0.1 mag, and the knowledge on these objects is limited.

This paper presents a detailed investigation of fifteen high-amplitude ($V_{\rm amp} > 0.1$ mag) GDOR (referred to hereafter for convenience as HAGDOR = High-Amplitude Gamma DORadus) stars with survey data and our own observations, with the aim of unraveling the mechanisms behind the observed high amplitudes and investigating possible systematic differences between the group of the regular ($V_{\rm amp} \leq 0.1$ mag) GDOR stars and the HAGDORs.

2 TARGET STARS AND ASTROPHYSICAL PARAMETERS

2.1 Target selection

The VSX was chosen as first source for selecting our initial sample stars as it is the most current and accurate variable star data base available. At the time of this writing, it listed a total of 24 GDOR stars out of 924 stars with amplitudes exceeding 0.1 mag – including KIC 8113425, which was analysed in detail by Kurtz et al. (2015). Ten of these objects boasted suitable photometric time series data allowing further detailed analyses and were hence selected for our sample. The stars KIC 7448050, KIC 6953103, and KIC 7304385, erroneously listed in the VSX with amplitudes less than 0.1 mag, were subsequently identified as HAGDOR stars and also included into our sample. As these examples illustrate, we suspect that, on detailed analysis, more low-amplitude GDOR stars listed in the VSX will likely turn out to be HAGDOR stars. Amplitude determination in these objects, which often show pronounced beating effects in their light curves, is not easy and prone to errors. An investigation into this matter, however, is beyond the scope of this paper. Finally, two more HAGDORs (HD 33575 and HD 211394) were identified in a systematic search among unclassified variables of suitable spectral type in the VSX. Both objects exhibit very large peak-to-peak amplitudes of more than 0.3 mag (*V*). In total, our final HAGDOR sample consists of 15 stars showing light change amplitudes in excess of 0.1 mag (*V*). Table 1 provides essential data for these objects.

For the six HAGDOR stars having both broad-band *Kepler* (*Kp*) data and *V*-band data from the All-Sky Automated Survey for Supernovae (ASAS-SN; cf. Section 3), we calculated and compared semi-amplitudes in the different passbands and found that Amp(*V*) / Amp(*Kp*) = 1.08(5). Assuming a colour–amplitude ratio of ∼1.25 for GDOR stars (Handler & Shobbrook 2002) and employing the relations for the calibration of *Kp* magnitudes given by Brown et al. (2011), we estimate Amp(*V*) / Amp(*Kp*) = 1.065(20), in line with the above mentioned result. We have therefore adopted Amp(*V*) / Amp(*Kp*) = 1.07(3) for the purposes of this study.

Reduced peak-to-peak amplitudes in *Kepler* data are expected, as photometric pulsation amplitudes in early-type stars generally decrease with increasing wavelength, and the *Kepler* passband covers the wavelength range from 420–900 nm, with peak transmission at around 600 nm (cf. Section 3.3). As only one sample star boasts Transiting Exoplanet Survey Satellite *(TESS)* data (HD 17721), a similar estimation of the relationship between Amp(*V*) and Amp(*TESS*) was not possible. However, we expect that pulsation amplitudes will be even more reduced in the redder *TESS* passband (600–1000 nm; cf. Section 3.4). This is in line with the results of Antoci et al. (2019), who investigated DSCT and GDOR stars with *TESS* data and estimated that pulsation amplitudes derived from *TESS* data only reach 74(1) per cent of those derived from *Kepler* data. Using Amp(*V*) / Amp(*Kp*) = 1.07, we estimate Amp(*V*) / Amp(*TESS*) = 1.44(4). The response functions of the Johnson *V*, *Kepler,* and *TESS* passbands are shown in Fig. 1.

To investigate systematic differences between the groups of HAGDOR and GDOR variables, a control sample of regular GDOR stars was selected from the VSX using the following criteria: (a) light change amplitudes of $0.05 \leq V \leq 0.1$ mag, (b) the availability of high-precision photometric time series data of suitable length that allow an in-depth analysis, (c) the availability of reliable astrophysical parameters, and (d) similar effective temperatures to the HAGDOR stars. The lower amplitude limit (a) was chosen because of the limitations of the employed ground-based photometric time series data (cf. also Section 3). Most GDOR stars in VSX have listed amplitudes that fail to satisfy criterion (a); therefore only 20 stars were selected. The stars of the regular GDOR sample can be gleaned from the lower part of Table 2.

2.2 Astrophysical parameters

Gaia DR2 (Gaia Collaboration et al. 2016, 2018; Arenou et al. 2018) includes effective temperatures, luminosities, and reddening values for nearly all our sample stars. As a first step, we checked the reliability of these parameters.

Effective temperatures were gleaned from the literature (Ammons et al. 2006; McDonald, Zijlstra & Boyer 2012; Pinsonneault et al. 2012; Huber et al. 2014; Munari et al. 2014; De Cat et al. 2015; Frasca et al. 2016; Kunder et al. 2017), and mean values and standard errors were calculated. Unfortunately, for one HAGDOR star (GSC 02831–00348), no parameters are available in the above-listed references. Reddening values were interpolated using the maps published by Green et al. (2018). Distances and their errors were derived from Gaia DR2 parallax data. Almost all our sample stars are located within 1 kpc from the Sun. Therefore, reddening is small but not negligible ($A_{\rm V} < 0.2$ mag). The only exception is the GDOR star GSC 04281–00186, which is located in the Galactic disc ($l = -0.45^{\circ}$).

To calculate luminosities of our sample stars, bolometric corrections (BC) and relative magnitudes *V* were needed. BC values are

[1]In this paper, unless indicated otherwise, amplitude always refers to peak-to-peak amplitude.

Table 1. Essential data for the sample HAGDOR stars, listed in order of increasing right ascension.

(1) Object	(2) Alternative ID	(3) RA (J2000)	(4) Dec. (J2000)	(5) Amp. (Source)	(6) Main per. (d)	(7) Spec. Type (lit)
GSC 02831–00348	V0758 And	02 22 20.479	+37 59 05.107	0.19 (A)	0.924655	n/a
HD 17721	HIP 13089	02 48 15.087	−57 39 42.498	0.14 (A3), 0.144 (T)	1.087858	A9 V (Houk & Cowley 1975)
HD 33575	NSV 1858	05 10 21.600	−23 13 01.950	0.35 (A3), 0.35 (A)	1.293260	A9 V (Houk & Smith-Moore 1988)
HD 50875	NSV 3272	06 54 33.947	−11 23 29.468	0.22 (A3)	1.705329	F2 V (Wright et al. 2003)
HD 85693	NSV 18291	09 52 56.364	−26 45 20.219	0.17 (A3)	1.125952	F0 V (Houk 1982)
GSC 09046–00646	ASAS J163451-6446.3	16 34 50.969	−64 46 18.299	0.21 (A3), 0.19 (A)	1.180647	n/a
HD 150538	NSV 20738	16 41 29.100	+06 16 33.387	0.21 (A3)	1.386903	F5 (Ochsenbein 1980)
KIC 3847822	TYC 3134-2121-1	19 22 57.126	+38 58 18.167	0.16 (A), 0.169 (K)	1.204964	n/a
KIC 3441414	GSC 03134–00901	19 23 21.727	+38 32 58.614	0.10 (A), 0.122 (K)	0.810700	F0 V (Gray et al. 2016)
KIC 7448050	ASAS J193103+4302.1	19 31 03.390	+43 02 06.368	0.19 (A), 0.182 (K)	0.877616	A9 IV-V (Gray et al. 2016)
KIC 6953103	2MASS J19325124+4228465	19 32 51.238	+42 28 46.505	0.24 (A), 0.249 (K)	0.776640	F0 V (this work)[1]
KIC 8113425	2MASS J19474808+4354257	19 47 48.082	+43 54 25.727	0.14 (A), 0.164 (K)	2.325268	F0 V (Frasca et al. 2016)
KIC 7304385	ASAS J195052+4248.1	19 50 51.541	+42 48 06.015	0.14 (A), 0.146 (K)	0.787874	F5 (Skiff 2014)
HD 211394	BD–17 6481	22 16 57.007	−16 59 03.156	0.32 (A3), 0.29 (R), 0.324 (K)	2.210397	F0 V (Bourgés et al. 2014)
GSC 02780–02174	TYC 2780-2174-1	23 51 25.338	+37 10 27.924	0.13 (A)	0.943619	F0 V (this work)[1]

[1]Derived from analysis of a publicly available LAMOST DR4 spectrum (Cui et al. 2012; Zhao et al. 2012) .The columns denote: (1) conventional identifier; (2) alternative identification; (3) right ascension (J2000); (4) declination (J2000); (5) peak-to-peak amplitude; the corresponding data source is provided in parentheses (A=ASAS-SN/A3=ASAS-3/K=*Kepler*/R=ROAD/T=*TESS*); (6) main period (d); (7) most recent spectral type from the literature. Positional information was taken from Data Release 2 (DR2) of the *Gaia* satellite mission (Gaia Collaboration et al. 2016, 2018; Arenou et al. 2018). Information on the relationship of the amplitudes in the different passbands can be gleaned from Section 2.1.

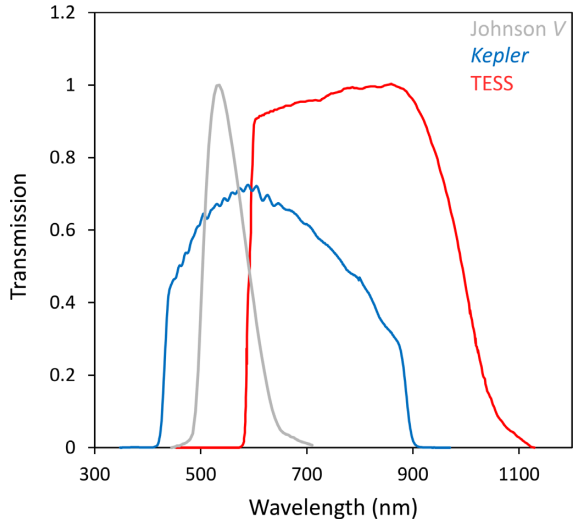

Figure 1. Response functions of the Johnson *V*, *Kepler,* and *TESS* passbands. Data have been gleaned from Johnson & Morgan (1951), Ricker et al. (2014), and the *Kepler* Instrument Handbook (https://keplerscience.arc.nasa.gov/).

at a minimum for F-type stars (Pecaut & Mamajek 2013) and do not significantly influence the luminosity calculation. Unfortunately, no homogeneous source of *V* magnitudes is available for all our target stars. Therefore, mean values of the magnitudes published by Kharchenko (2001) and Henden et al. (2016) were calculated and *G* magnitudes from Gaia DR2 were transformed. The final mean astrophysical parameters are listed in Table 2.

Fig. 2 shows a comparison between the values derived in this paper and the values derived from Gaia DR2. It becomes obvious that the *Gaia* reddening values are significantly larger than those derived from the reddening maps (upper panel). As a consequence, the corresponding luminosities are lower than the luminosities calibrated with the parallax data and the other observables (lower panel). The situation for the effective temperatures (middle panel) is different. With only three exceptions, all stars are located on the unity line within the errors. For each of the three outliers, only one effective temperature value is available in the literature. Therefore, it is not possible to investigate the reason for, and estimate the significance of, the outlying positions in the diagram. In consequence, for the following analyses, we have employed our own luminosity values and effective temperatures from Gaia DR2 because the latter have been derived in a homogeneous way.

Fig. 3 presents the $\log T_{\rm eff}$ versus $\log L/L_{\odot}$ diagram of our sample stars. Also shown are the GDOR (Dupret et al. 2004) instability strip and the red border of the DSCT (Breger & Pamyatnykh 1998) instability strip. No obvious differences are seen between the location of the GDOR and HAGDOR stars; both groups are well distributed over the whole main sequence up to $\log L/L_{\odot} < 1.1$. Interestingly, most stars are also located in the DSCT instability strip but do not show any corresponding pulsations with a detectable amplitude in the here employed photometric time series data.

Two objects deserve mention, which are situated well outside the instability strips. These are the GDOR stars GSC 04281–00186 and GSC 09289–02186. According to its calibrated astrophysical parameters, GSC 09289–02186 is a G0 V star. GSC 04281–00186 is apparently a G-type giant situated in a significantly reddened ($A_{\rm V} = 1.4$ mag) region at a Galactic latitude of $b \approx 0°$. Nevertheless, even when neglecting reddening, we find the star still far above the terminal-age main sequence. Using the standard reddening correlation $A(V) = 3.45A(J) = 5.89A(H) = 7.69A(K_{\rm s})$ (Paunzen, Netopil & Herdin 2017), the derived indices $(J - H)_0 = -0.115$ mag and $(H - K_{\rm s})_0 = +0.040$ mag are typical for an early B-type star (Straižys & Lazauskaitė 2009). However, Gaia DR2 colours (and all others in the optical region) are typical for a G-type object. Also, the derived effective temperature from Gaia DR2 is in agreement with all other published values. The star's status as an evolved object therefore seems to be beyond doubt. This is intriguing as giant stars are not expected to exhibit GDOR pulsation. Both objects are further discussed in Section 4.3.

Table 2. Mean astrophysical parameters of our target stars. The upper part of the table contains the HAGDOR stars, the lower part the GDOR stars.

(1) Object	(2) Alternative ID	(3) A_V (our)	(4) A_G (DR2)	(5) BC (our)	(6) V (our)	(7) log $T_{\rm eff}$ (our)	(8) log $T_{\rm eff}$ (DR2)	(9) log $L/L_\odot$ (our)	10 log $L/L_\odot$ (DR2)
GSC 02831–00348	V0758 And	0.11	0.55(39)	+0.00	11.390(4)	–	3.883(20)	0.80(3)	0.78(2)
HD 17721	HIP 13089	0.00	0.56(35)	−0.01	8.598(1)	3.852(5)	3.855(8)	0.78(2)	0.77(1)
HD 33575	NSV 1858	0.05	0.78(26)	−0.01	9.708(2)	3.866	3.855(8)	0.84(2)	0.82(1)
HD 50875	NSV 3272	0.08	0.69(28)	−0.01	8.521(2)	3.853	3.852(9)	0.87(2)	0.83(1)
HD 85693	NSV 18291	0.03	–	−0.01	7.679(2)	3.839(1)	3.845(14)	0.92(2)	0.90(1)
GSC 09046–00646	ASAS J163451–6446.3	0.22	0.62(31)	−0.01	10.251(2)	3.822	3.843(6)	0.89(2)	0.80(1)
HD 150538	NSV 20738	0.22	1.08(29)	−0.02	9.731(2)	3.830(28)	3.839(13)	1.02(2)	0.93(1)
KIC 3847822	TYC 3134-2121-1	0.14	0.63(19)	−0.01	11.866(1)	3.850(1)	3.861(16)	0.76(2)	0.72(1)
KIC 3441414	GSC 03134–00901	0.16	0.48(38)	−0.01	11.539(2)	3.855(11)	3.854(8)	0.83(3)	0.77(1)
KIC 7448050	ASAS J193103+4302.1	0.11	0.62(24)	−0.01	11.838(2)	3.861(14)	3.860(8)	0.79(2)	0.76(1)
KIC 6953103	2MASS J19325124+4228465	0.19	0.36(26)	−0.01	12.593(2)	3.854(11)	3.855(11)	0.75(3)	0.68(2)
KIC 8113425	2MASS J19474808+4354257	0.47	1.35(11)	−0.04	13.931(1)	3.841(8)	3.820(16)	0.85(3)	0.67(3)
KIC 7304385	ASAS J195052+4248.1	0.14	0.78(25)	−0.01	10.078(1)	3.847(18)	3.843(14)	0.85(2)	0.80(1)
HD 211394	BD–17 6481	0.08	1.29(22)	−0.04	9.306(3)	3.826(9)	3.822(3)	0.97(3)	0.92(1)
GSC 02780–02174	TYC 2780-2174-1	0.30	0.92(29)	−0.02	11.754(2)	3.785	3.835(10)	0.78(3)	0.66(1)
HD 18011	HIP 13494	0.14	0.55(17)	−0.01	9.201(1)	3.852(10)	3.851(12)	0.84(2)	0.78(1)
CD–87 32	TYC 9500-1039-1	0.13	–	−0.03	10.283(1)	3.841	3.827(17)	0.88(2)	0.82(1)
BD–12 1502	NSV 16873	0.11	0.59(23)	−0.01	8.937(1)	3.848(4)	3.850(10)	0.81(2)	0.76(1)
EPIC 202072613	TYC 1342-1962-1	0.03	0.12(18)	0.00	11.276(1)	3.852	3.873(6)	0.66(2)	0.67(1)
CD–23 9345	TYC 6620-698-1	0.08	0.47(24)	−0.01	10.018(2)	3.837(10)	3.856(11)	0.81(2)	0.78(1)
HD 124248	MU Vir	0.00	0.38(26)	−0.01	7.156(2)	3.862(6)	3.851(10)	0.78(2)	0.77(1)
HD 135825	IN Lib	0.00	0.40(22)	−0.01	7.285(2)	3.854(13)	3.851(13)	0.74(2)	0.72(1)
GSC 08298–00090	TYC 8298-90-1	0.50	0.82(39)	−0.04	11.214(2)	3.826	3.815(6)	0.86(2)	0.65(1)
GSC 09289–02186	V0366 Aps	0.20	–	−0.09	11.522(1)	3.814	3.775(5)	0.86(2)	0.76(1)
HD 164615	V2118 Oph	0.00	–	−0.01	6.995(1)	3.849(14)	3.842(9)	0.86(2)	0.85(1)
KIC 12643786	TYC 3554-1916-1	0.08	0.59(40)	+0.00	11.470(1)	3.855(18)	3.877(19)	0.88(2)	0.82(1)
KIC 11080103	2MASS J19185013+4837138	0.14	0.61(22)	+0.00	12.875(1)	3.867(13)	3.885(17)	0.85(3)	0.77(2)
KIC 5105754	TYC 3139-2577-1	0.16	0.53(42)	−0.01	11.355(1)	3.847(11)	3.852(6)	0.88(2)	0.77(1)
KIC 4757184	TYC 3139-499-1	0.19	–	+0.00	11.777(1)	3.875(24)	3.871(9)	1.01(3)	0.91(2)
KIC 11920505	TYC 3564-2927-1	0.05	0.48(30)	−0.01	9.772(1)	3.836(13)	3.856(8)	0.79(2)	0.73(1)
KIC 11826272	BD+49 3115	0.19	0.78(26)	−0.01	10.294(2)	3.852(22)	3.844(7)	0.94(2)	0.82(1)
HD 187615	V1844 Aql	0.03	0.55(22)	−0.01	7.939(1)	3.861(6)	3.854(10)	0.80(2)	0.78(1)
GSC 09086–01560	TYC 9086-1560-1	0.19	0.55(17)	+0.00	11.229(2)	3.874(2)	3.871(9)	0.85(3)	0.79(1)
HD 218225	DI Gru	0.09	–	−0.01	8.724(1)	3.846(8)	3.849(10)	0.98(2)	0.93(1)
GSC 04281–00186	TYC 4281-186-1	1.40	1.65(40)	−0.08	11.276(1)	3.757	3.783(7)	1.98(3)	1.40(2)

The columns denote: (1) conventional identifier; (2) alternative identification; (3,4) absorption in V and G; (5) BC, (6) V magnitude and error; (7,8) logarithmic effective temperature and error estimate; (9,10) logarithmic luminosity and error estimate.

3 DATA SOURCES AND METHOD OF ANALYSIS

3.1 The ASAS-3 photometric archive

Phase 3 of the All Sky Automated Survey (ASAS-3) lasted from 2000 until 2009 (Pojmański 2002) and monitored the entire southern sky and part of the northern sky ($\delta < +28^\circ$). The ASAS-3 system was situated at the 10-inch astrograph dome of the Las Campanas Observatory in Chile and boasted two wide-field telescopes equipped with f/2.8 200 mm Minolta lenses and 2048 x 2048 AP 10 Apogee detectors. About 10^7 sources were monitored in the Johnson V passband. The ASAS-3 archive contains photometry for stars in the magnitude range $7 \lesssim V \lesssim 14$; the most accurate photometry was obtained for stars in the range of $8 \lesssim V \lesssim 10$, boasting a typical scatter of about 0.01 mag (Pigulski 2014).

The long time baseline of almost 10 yr renders the detection of periodic signals with very small amplitudes possible. For instance, David, Hensberge & Nitschelm (2014) identified periodic variables with a peak-to-peak amplitude of 0.01–0.02 mag in the magnitude range of $7 \lesssim V \lesssim 10$. According to Pigulski (2014), the detection of periodic signals in the frequency range of $0 < f(\mathrm{d}^{-1}) < 40$ with amplitudes as low as about 5 mmag is possible.

3.2 The ASAS-SN photometric archive

The ASAS-SN survey is monitoring the entire visible sky every night to a depth of $V \lesssim 17$ mag (Shappee et al. 2014; Kochanek et al. 2017). The available data span up to 6 yr of observations. As of end-2017, ASAS-SN observations are procured at five stations, each consisting of four 14 cm aperture Nikon telephoto lenses. Observations consist of three dithered 90 s exposures made through V (two stations) or g (three stations) band filters. ASAS-SN saturates at 10–11 mag, where the exact limit depends on the camera and the image position (vignetting). However, a procedure inherited from the original ASAS survey is applied which corrects for saturation but increases the noise in the affected data sets (Jayasinghe et al. 2018).

3.3 The *Kepler* satellite photometric archive

The *Kepler* satellite was launched in 2009 March, with the primary goal of detecting transiting exoplanets in the solar neighbourhood. The space-based photometer has a 0.95 m aperture; the detectors consist of 21 modules each equipped with two 2200 x 1024 pixel CCDs. *Kepler* provides single passband (420–900 nm; Koch et al.

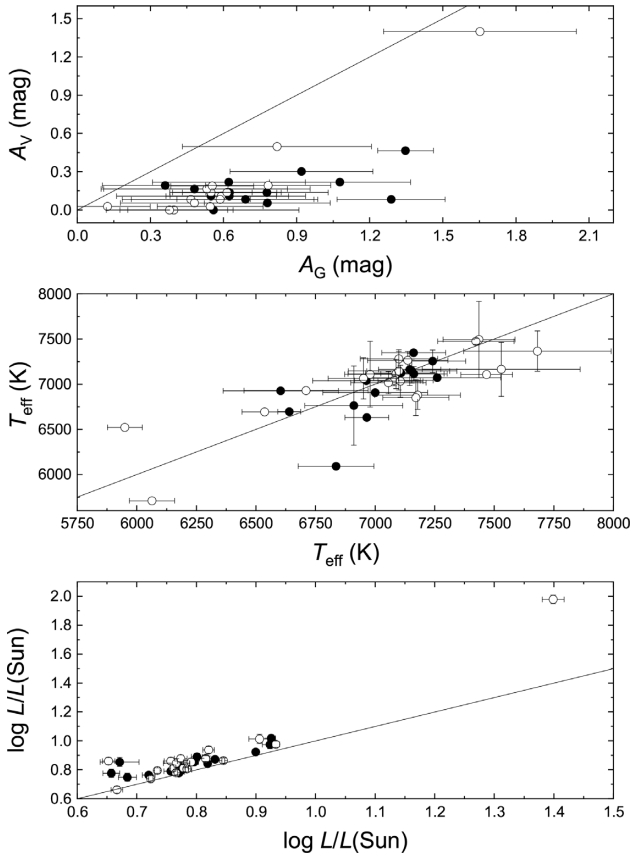

Figure 2. Comparison of the reddening (upper panel), effective temperature (middle panel), and luminosity (lower panel) values derived in this paper (ordinate values; Table 2) and from GAIA DR2 (abscissa values). Filled and open circles denote HAGDOR and GDOR stars, respectively. Also indicated are the unity lines.

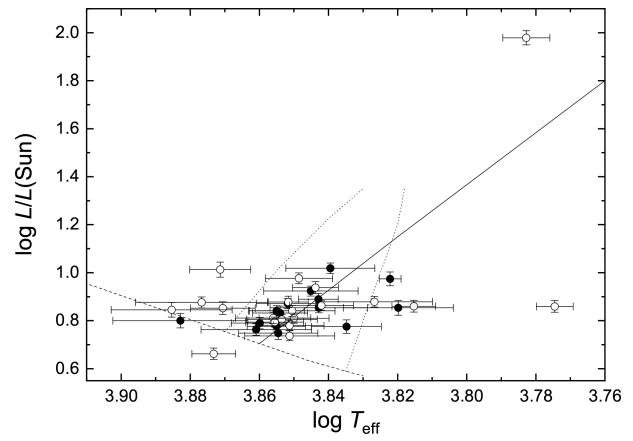

Figure 3. The $\log T_{\rm eff}$ versus $\log L/L_{\odot}$ diagram of our programme stars (Table 2). The red border of the DSCT (solid line), and the GDOR (dotted lines) instability strips are taken from Breger & Pamyatnykh (1998) and Dupret et al. (2004), respectively. The zero-age main sequence (dashed line) is taken from Claret (1995). Filled and open circles denote HAGDOR stars and GDOR stars, respectively.

2010) light curves of micromagnitude precision, taken in long-cadence (29.5 min) and short-cadence (58.5 s) modes (Gilliland et al. 2010), and has discovered hundreds of planet candidates (Borucki et al. 2010). The long, uninterrupted, and high-precision time series photometry is ideally suited to the study of multiperiodic pulsating stars (Tkachenko et al. 2012).

3.4 The *TESS* satellite photometric archive

The Transiting Exoplanet Survey Satellite (*TESS*) mission is a 2-yr all-sky survey aiming at the discovery of transiting exoplanets (Ricker et al. 2015). To this end, four MIT/Lincoln Lab CCDs with 4096 x 4096 pixels are employed (imaging area of 2048 x 2048 pixels; the remaining pixels are used as a frame-store to allow rapid shutterless readout). The cameras have an effective aperture size of 10 cm and are equipped with f/1.4 lenses, resulting in a field of view of 24° x 24° per camera. The *TESS* passband covers the wavelength range from about 600–1000 nm. Due to their high photometric precision, time sampling of 2 min and long intervals of uninterrupted observations, *TESS* data are well suited to asteroseismology (Campante et al. 2016).

3.5 The Remote Observatory Atacama Desert (ROAD)

New CCD photometric observations of one target (HD 211394) were acquired at the Remote Observatory Atacama Desert (ROAD; Hambsch 2012). All observations were acquired through an Astrodon Photometric *V* filter with an Orion Optics, UK Optimized Dall Kirkham 406/6.8 telescope, and a FLI 16803 CCD camera. The exposure time was 5 s; twilight sky-flat images were used for flat-field corrections. Reductions were performed with the MAXIM DL programme.[2] For the determination of magnitudes, the LESVEPHOTOMETRY program[3] was employed.

3.6 Method of analysis

The data of our target stars were downloaded from the ASAS-3 website,[4] the ASAS-SN archive[5], and, in the case of *Kepler* and *TESS* data, the Mikulski Archive for Space Telescopes (MAST).[6] All light curves were inspected visually. Obvious outliers and data points with very large uncertainties were carefully removed. In the case of the ASAS-3 data, measurements with a quality flag of 'D' (='worst data, probably useless') were deleted.

The time of the ASAS-3 and ASAS-SN observations are provided in HJD-2450000. *Kepler* and *TESS* data, however, are formatted as BJD-2454833 and BJD-2457000, respectively. To facilitate analysis, *Kepler* and *TESS* data were converted to HJD-2450000 to bring them in line with the ground-based data.[7]

The period analysis was done using the program package PERIOD04 (Lenz & Breger 2005), which employs discrete Fourier transform and allows least-squares fitting of multiple frequencies to the data. To extract all relevant frequencies, the data were searched for periodic signals and consecutively pre-whitened with the most significant frequencies. As detection threshold, we adopted S/N $\geq$ 4 (Breger et al. 1993).

[2] http://www.cyanogen.com
[3] http://www.dppobservatory.net/
[4] http://www.astrouw.edu.pl/asas/
[5] https://asas-sn.osu.edu/
[6] https://archive.stsci.edu/access-mast-data
[7] In all cases, the calculation of the phase values provided in the presentation of results has been based on the time basis of HJD-2450000.

4 PRESENTATION AND DISCUSSION OF RESULTS

In this section, we present example results and discuss the light variability patterns of the HAGDOR variables on the basis of the HAGDOR star KIC 8113425, which has been extensively studied by Kurtz et al. (2015) and is here employed as a model case.

4.1 The HAGDOR star KIC 8113425 as a model case

In their investigation of the complex frequency spectra of GDOR, Slowly Pulsating B stars and Be stars, Kurtz et al. (2015) extensively studied the HAGDOR star KIC 8113425. It has therefore been employed as a model case for a general interpretation of the light variations of our sample HAGDOR stars which also include KIC 8113425. Kurtz et al. (2015) noted the complex, strongly non-linear light variations of this star, which shows a much larger range at maximum light than minimum light (type ASYM) and identified 43 frequencies with semi-amplitudes greater than 1 mmag that cluster in five frequency groups. All these 43 frequencies can be understood in terms of only four base frequencies ($f_1 = 0.430058\,\mathrm{d}^{-1}$, $f_2 = 0.450101\,\mathrm{d}^{-1}$, $f_3 = 0.461264\,\mathrm{d}^{-1}$, and $f_4 = 0.489414\,\mathrm{d}^{-1}$) and their combination frequencies up to the order $2f$ (e.g. $2f_1$, $f_2 + f_3 - f_4$). To trace and investigate the results of Kurtz et al. (2015), simulated light curves were calculated based on the frequency and phase information provided by the aforementioned authors.

The full *Kepler* light curve of KIC 8113425 and a detailed view are shown in the top panels of Fig. 4. The other panels of this figure illustrate the simulated light curves using

(a) all 43 frequencies,
(b) 7 frequencies (4 base frequencies and the 3 detected overtone frequencies $2f_1$, $2f_3$, and f_4),
(c) 4 frequencies (the base frequencies), and
(d) 1 frequency (f_1, the frequency with the largest semi-amplitude, 0.01455 mag).

We have investigated the contribution of the corresponding frequencies to the total variability amplitude. The base frequency f_1 with its peak-to-peak amplitude of 0.028 mag accounts for only ∼21 per cent of the total amplitude (0.137 mag) of the observed light variations. The four base frequencies together add up to an amplitude of about 0.076 mag (∼55 per cent of the total amplitude), while the four base frequencies plus the three overtone frequencies reach an amplitude of 0.0858 mag (∼62 per cent). The 43 frequencies add up to an amplitude of 0.109 mag, which is ∼80 per cent of the total amplitude. According to the conclusions of Kurtz et al. (2015), suitable combination frequencies can result in considerably larger peak-to-peak amplitudes than the base frequency alone, as has been shown above. This is in agreement with the finding that, apart from these special cases, GDOR variables usually show low amplitudes.

4.2 Light variability pattern of the other HAGDOR variables

Eight stars of our sample boast satellite photometry from *Kepler* or *TESS* that allow a similarly detailed analysis. For the remaining seven objects with only ground-based observations, however, the precision and number of available measurements is not sufficient to perform an analysis of a vast number of frequencies. Nevertheless, it becomes obvious that all of our sample HAGDOR stars exhibit multiperiodic variability in a similar way to KIC 8113425: in all objects, the beating of closely spaced frequencies results in total amplitudes that considerably exceed the amplitudes of the base frequencies. This leads to the observed 'upward trends' in the light curves, as described in Kurtz et al. (2015) and clearly seen, for example, in the

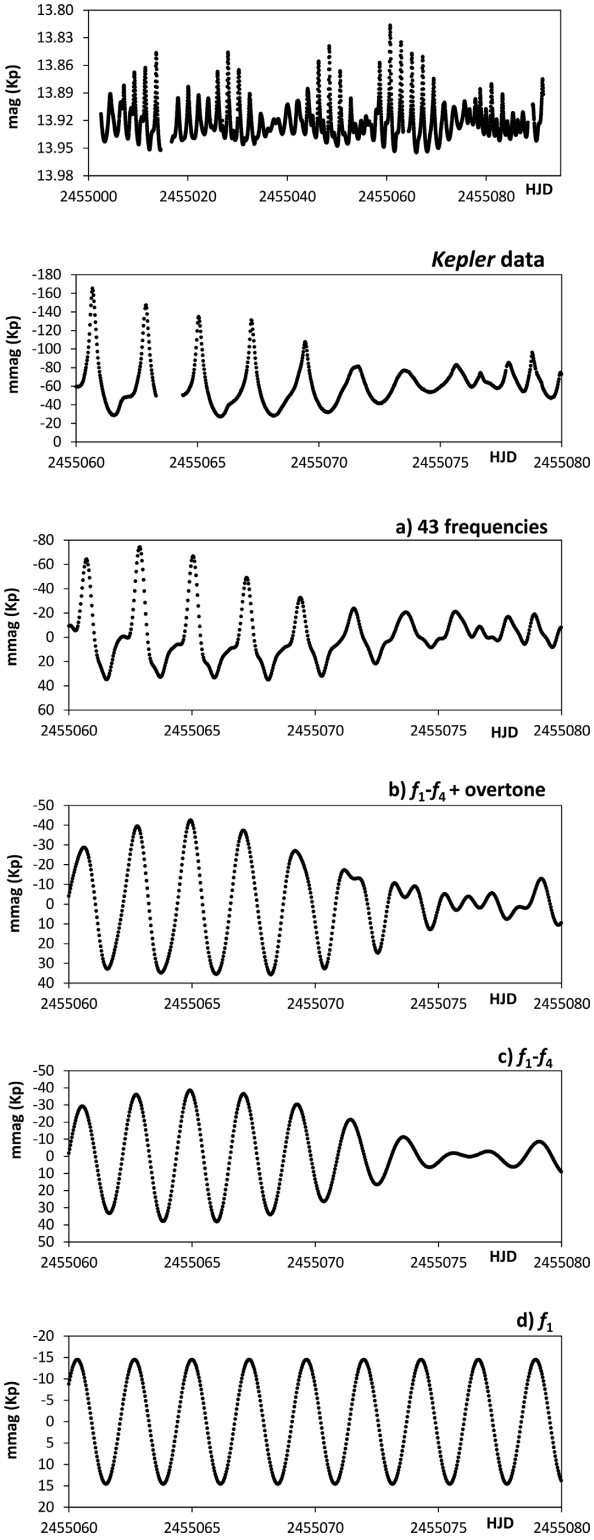

Figure 4. The two top panels show the full *Kepler* light curve of KIC 8113425 and the light curve in the interval HJD 2455060–80. The other panels illustrate the simulated light curves using (a) 43 frequencies, (b) 7 frequencies, (c) 4 frequencies, and (d) 1 frequency, as described in Kurtz et al. (2015).

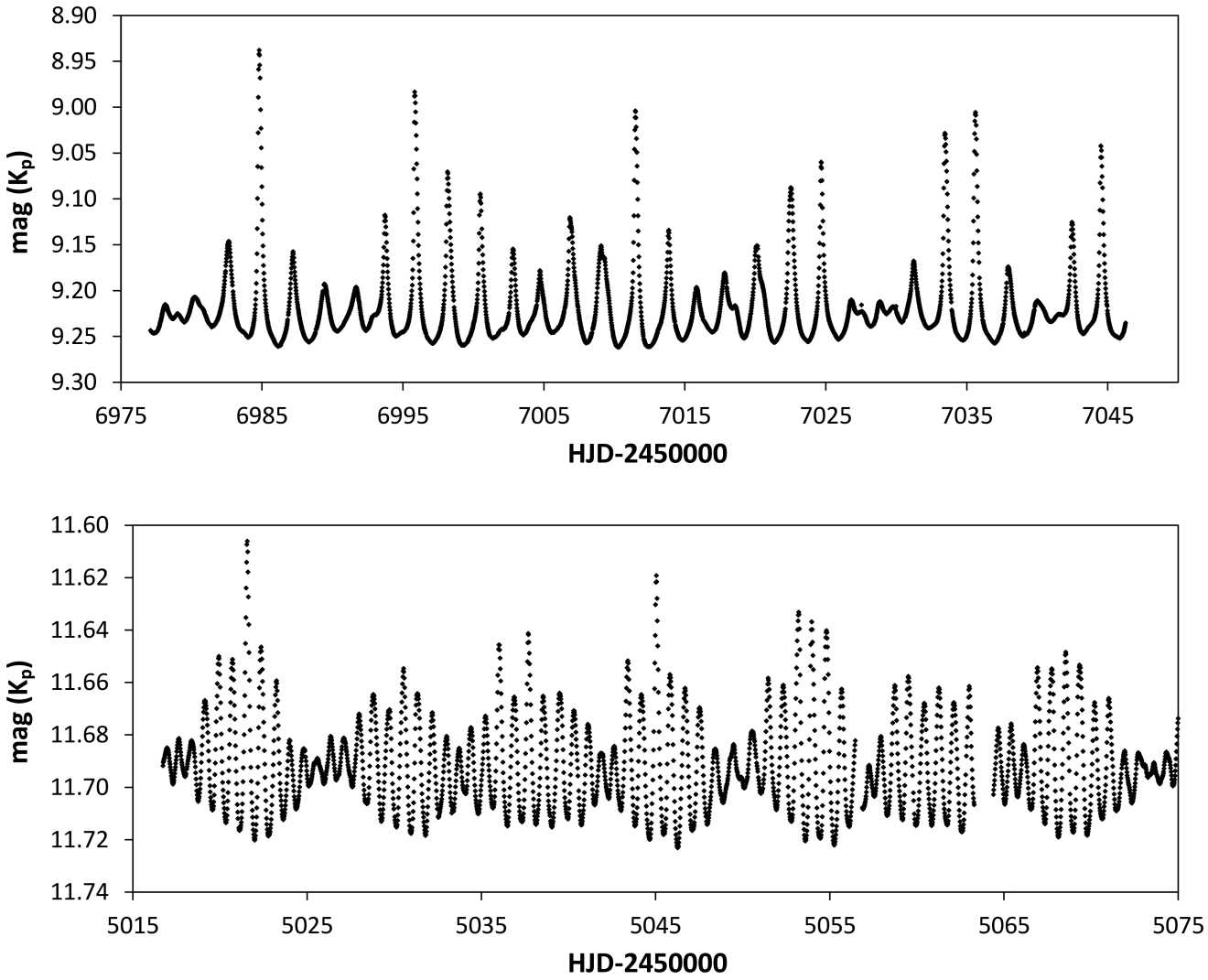

Figure 5. Detailed view of parts of the *Kepler* light curves of HD 211394 (upper panel) and KIC 3441414 (lower panel), highlighting the beating effects in the light curves and the high peak-to-peak amplitudes of 0.324 and 0.122 mag, respectively. Both stars show light curves of the ASYM type (Balona et al. 2011).

light curves of KIC 8113425 (Fig. 4, upper panel), HD 211394, and KIC 3441414 (both Fig. 5). These upward trends can, for example, arise if the phase difference of the second harmonic in relation to the base frequency is nearly zero, as has been observed for f_4 in KIC 8113425. Similar upward trends are clearly present in the light curves of all other investigated HAGDOR variables, although in ASAS-3 and ASAS-SN data, these are sometimes only represented by a 'smattering' of bright data points around the time of maximum light in the phase diagrams. All HAGDOR stars therefore belong to the ASYM group of Balona et al. (2011; cf. also Section 4.3).

As examples, Fig. 5 illustrates the *Kepler* light curves of the two HAGDOR stars HD 211394 and KIC 3441414. The large peak-to-peak amplitudes of the observed variations (0.324 and 0.122 mag, respectively) become directly obvious. HD 211394, in particular, is noteworthy because it is one of the stars with the largest amplitude in our sample. Using Amp(V) / Amp(Kp) = 1.07(3) (cf. Section 2.1), its light variations reach a peak-to-peak amplitude in V of about 0.35 mag, which is only rivalled by the variability of HD 33575 (Amp(V) = 0.35 mag).

The corresponding Fourier amplitude spectra are shown in Fig. 6, the frequency solutions, as derived from the different data sources, are presented in Tables 3 and 4 . Fig. 6 also illustrates the higher noise level, lower sampling rate, and the presence of one-day alias peaks in the ground-based ASAS-3 and ASAS-SN data. Nevertheless, these data span a much longer time baseline and are still very much suitable for the goals of the present investigation, which is also demonstrated by the good agreement between the principal frequencies derived from the different data sources. We also note that pulsation amplitudes are higher in V than in the broad-band *Kepler* and *TESS* data, which can also be seen in Fig. 6 (cf. Section 2.1).

The frequency solutions for all stars are shown in the Appendix in Tables A1–A15. Fourier amplitude spectra of all HAGDOR stars are presented in Fig. B1.

In summary, we conclude that the observed high amplitudes in the HAGDOR stars are caused by the presence of multiple, closely spaced frequencies and their interactions. In this way, although the maximum amplitude of the primary frequencies does not exceed an amplitude of 0.1 mag, total light variability amplitudes of over 0.3 mag (V) can be attained, as for example, in the case of HD 211394 and HD 33575. This is an interesting result that shows the need for the revision of the customary GDOR star class definition and provides important input for pulsational modelling attempts.

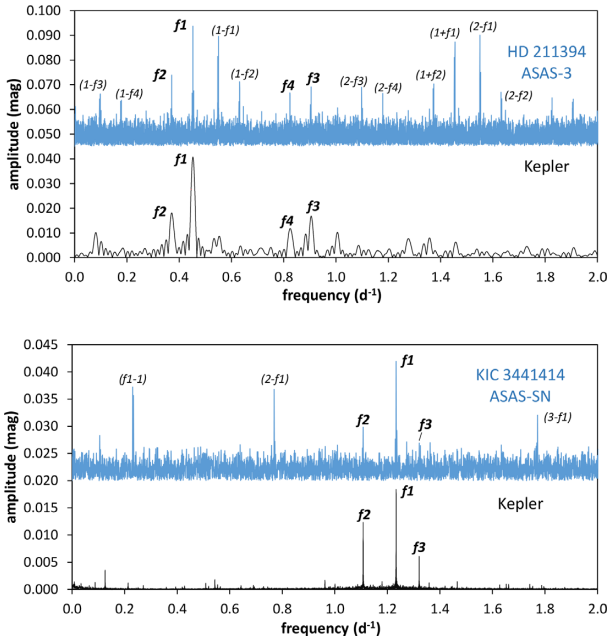

Figure 6. Fourier amplitude spectra of HD 211394, based on unwhitened ASAS-3 and *Kepler* data (upper panel), and KIC 3441414, based on unwhitened ASAS-SN and *Kepler* data (lower panel). Note the presence of numerous alias peaks (identified using brackets) in the ground-based data.

Table 3. Frequency solution for *HD 211394*.

(1) Frequency number	(2) Frequency	(3) Amplitude	(4) Phase	(5) ID
$F1_{\mathrm{ASAS\text{-}3}}$	0.452407	0.049	0.7275	f_1
$F2_{\mathrm{ASAS\text{-}3}}$	0.371387	0.027	0.6153	f_2
$F3_{\mathrm{ASAS\text{-}3}}$	0.904804	0.020	0.7111	$2f_1$
$F4_{\mathrm{ASAS\text{-}3}}$	0.823776	0.018	0.6548	f_1+f_2
$F5_{\mathrm{ASAS\text{-}3}}$	1.276179	0.014	0.6848	f_2+2f_1
$F1_{\mathrm{ROAD}}$	0.452625	0.051	0.0744	f_1
$F2_{\mathrm{ROAD}}$	0.370860	0.026	0.7140	f_2
$F3_{\mathrm{ROAD}}$	0.823041	0.020	0.4374	f_1+f_2
$F4_{\mathrm{ROAD}}$	0.904372	0.018	0.1150	$2f_1$
$F1_{\mathrm{Kepler}}$	0.452538	0.04193	0.8082	f_1
$F2_{\mathrm{Kepler}}$	0.372089	0.01975	0.7546	f_2
$F3_{\mathrm{Kepler}}$	0.905160	0.01774	0.2723	$2f_1$
$F4_{\mathrm{Kepler}}$	0.824686	0.01274	0.4111	f_1+f_2
$F5_{\mathrm{Kepler}}$	0.080533	0.01063	0.3164	f_1-f_2
$F6_{\mathrm{Kepler}}$	1.005225	0.01002	0.3856	f_3
$F7_{\mathrm{Kepler}}$	0.533652	0.00904	0.2196	$2f_1-f_2$
$F8_{\mathrm{Kepler}}$	1.357718	0.00816	0.2133	f_4

4.3 Comparison of the samples of GDOR and HAGDOR variables

Several studies have indicated that high-amplitude DSCT (HADS) stars are distinguished from the lower-amplitude DSCT variables by several criteria: they generally show only one or two excited radial modes (usually the fundamental mode and/or first harmonic) and are mostly slow rotators, which seems to be a requirement for the observed high-amplitude pulsation (Breger 2000; McNamara 2000). It has also been postulated that HADS stars are in an evolutionary stage that puts them between low-mass classical Cepheids and high-mass DSCT stars; however, in their investigation of the physical

Table 4. Frequency solution for *KIC 3441414*.

(1) Frequency number	(2) Frequency	(3) Amplitude	(4) Phase	(5) ID
$F1_{\mathrm{ASAS\text{-}SN}}$	1.233502	0.021	0.5729	f_1
$F2_{\mathrm{ASAS\text{-}SN}}$	1.107843	0.010	0.7617	f_2
$F3_{\mathrm{ASAS\text{-}SN}}$	1.321001	0.007	0.2928	f_3
$F1_{\mathrm{Kepler}}$	1.233479	0.01841	0.1633	f_1
$F2_{\mathrm{Kepler}}$	1.107875	0.01237	0.8904	f_2
$F3_{\mathrm{Kepler}}$	1.320999	0.00622	0.6805	f_3
$F4_{\mathrm{Kepler}}$	0.125600	0.00350	0.1636	f_1-f_2
$F5_{\mathrm{Kepler}}$	2.341354	0.00230	0.3444	f_1+f_2
$F6_{\mathrm{Kepler}}$	0.543345	0.00176	0.3657	f_4
$F7_{\mathrm{Kepler}}$	0.962388	0.00170	0.4148	f_5
$F8_{\mathrm{Kepler}}$	2.466959	0.00164	0.6123	$2f_1$
$F9_{\mathrm{Kepler}}$	1.465986	0.00138	0.7528	f_6
$F10_{\mathrm{Kepler}}$	0.087513	0.00134	0.4919	f_3-f_1
$F11_{\mathrm{Kepler}}$	1.179790	0.00130	0.4088	f_7
$F12_{\mathrm{Kepler}}$	0.213140	0.00120	0.6362	f_3-f_2
$F13_{\mathrm{Kepler}}$	0.508685	0.00109	0.6989	f_8
$F14_{\mathrm{Kepler}}$	1.661927	0.00109	0.3922	f_9
$F15_{\mathrm{Kepler}}$	1.742302	0.00108	0.0020	f_{10}
$F16_{\mathrm{Kepler}}$	1.359081	0.00105	0.6474	$2f_1-f_2$
$F17_{\mathrm{Kepler}}$	0.034023	0.00102	0.4082	$-2f_1+f_3+f_7$
$F18_{\mathrm{Kepler}}$	1.652501	0.00095	0.9946	$f_1-f_4+f_5$

nature of HADS stars using *Kepler* data, Balona et al. (2016) rejected this scenario and found that HADS stars are distributed randomly across the DSCT instability strip. No physical attribute was found that separates HADS stars from their low-amplitude counterparts, although there seems to be a general tendency for the number of combination frequencies to increase with increasing amplitude of the parent frequencies (Balona et al. 2016). Further investigation into the relationship between DSCT, HADS stars, and the related low-metallicity SX Phe stars is clearly desirable.

Here, we investigate the relationship between HAGDOR and GDOR stars. Their locations in the instability strip (Fig. 3) and $\log T_{\mathrm{eff}}$ versus $\log L/L_{\odot}$ diagram (cf. Section 2.2) suggest that GDOR and HAGDOR stars are not physically distinct objects but rather a homogeneous group of variables. To further tackle this question, we have investigated the relation between the primary variability frequency and the parameters effective temperature and luminosity (Fig. 7). Both GDOR and HAGDOR stars overlap in the investigated parameter spaces and no significant correlation was found. The situation is similar for the semi-amplitudes of the primary frequencies: although HAGDOR stars tend to show larger amplitudes, as expected, no distinct boundary between GDOR and HAGDOR stars is observed but rather a gradual transition and considerable overlap. We have also correlated the two most significant frequencies and their corresponding semi-amplitudes (Fig. 7, right-hand panels). Again, while HAGDOR stars tend to show larger amplitudes, no significant differences were found between the two investigated groups. Interestingly, nearly all of the investigated stars show closely spaced primary frequencies, which seems to be a characteristic of the class of GDOR variables.

It is interesting to point out, though, that all HAGDOR stars have light curves of the ASYM type, whereas the control sample of GDORs is predominately made up of stars having SYM light curves. The occurrence of the characteristic beating effects observed in the ASYM group therefore seems to be necessary for the development of the high variability amplitudes observed in the HAGDOR stars.

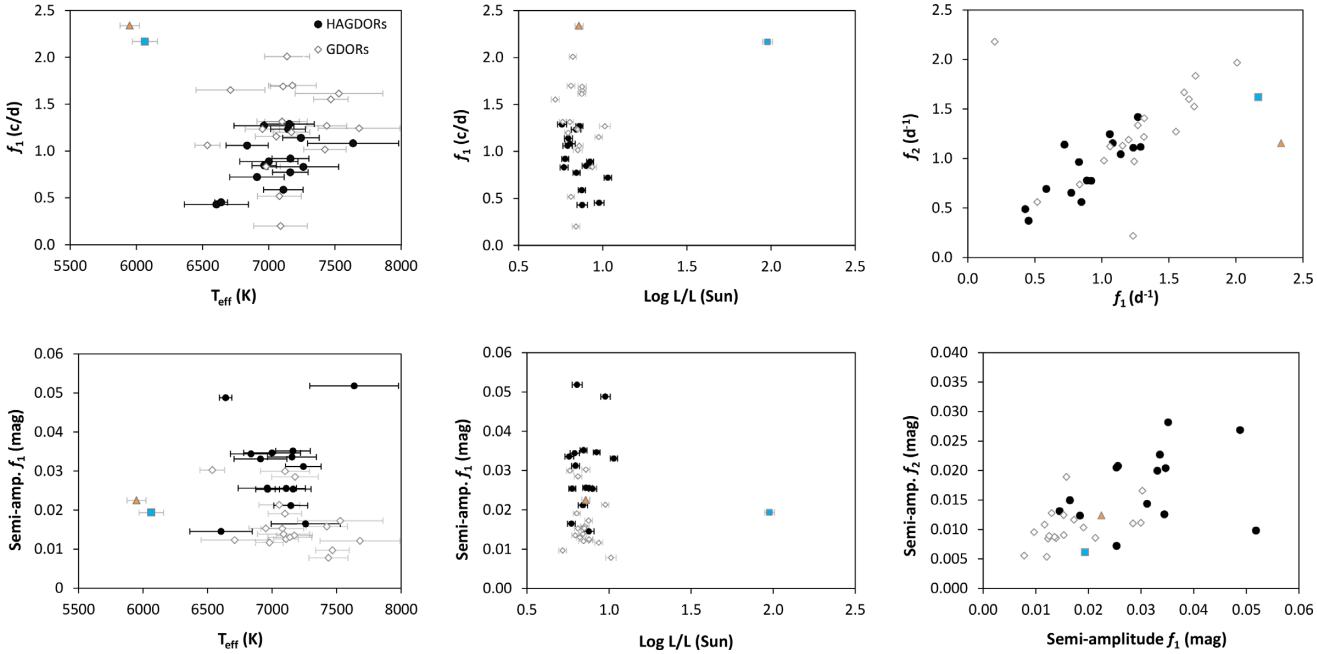

Figure 7. Correlations between several observables for the sample of HAGDOR stars (black circles) and GDOR stars (open diamonds). The GDOR stars GSC 09289–02186 and GSC 04281–00186 are indicated, respectively, by an orange triangle and a blue rectangle in all plots. The panels investigate primary frequency versus effective temperature (upper left-hand panel), semi-amplitude of the primary frequency versus effective temperature (lower left-hand panel), primary frequency versus luminosity (upper middle panel), semi-amplitude of the primary frequency versus luminosity (lower middle panel), the correlation between the two most significant frequencies (upper right-hand panel) and their corresponding semi-amplitudes (lower right-hand panel). There generally is no significant difference in distribution between HAGDOR and GDOR stars, which do not seem to be physically distinct in any other respect than their total variability amplitudes.

In summary, the here presented evidence – although based on rather small sample sizes – suggests that GDORs and HAGDORs are not physically distinct in any other respect than their total variability amplitudes but merely represent the low- and high-amplitude ends of the same, uniform group of variables, with a continuous progression from low to high total amplitudes.

The G0V star GSC 09289–02186 and the G-type giant GSC 04281–00186 (cf. Section 2.2), both belonging to the GDOR star sample, constitute the most obvious outliers in the diagrams presented in Fig. 7, in particular, in the primary frequency versus effective temperature plot (upper left-hand panel), and deserve special mention. These stars exhibit the characteristic variability patterns of GDOR stars and show light curves of the SYM type; however, both stars are situated outside the traditional boundaries of the GDOR realm, whose red border is found at a spectral type of approximately F7 (cf. Section 1). Furthermore, GDOR stars belong to luminosity classes IV or V by definition (Kaye et al. 1999). The case of a giant star exhibiting pulsation compatible with a GDOR type is therefore of interest.

Balona et al. (2011) noticed the occurrence of giant stars with $T_{\rm eff} < 6000$ K in their sample of GDOR stars with MULT-type light curves. They surmised that these objects represent solar-type oscillators among late G giants. However, the variability pattern of the giant star GSC 04281–00186, which is characterized by two main pulsations frequencies with rather high amplitudes (Fig. 8), is vastly different from the variability seen in solar-like pulsating stars, which show rich frequency spectra of stochastically excited modes (e.g. Bedding et al. 2010; Chaplin & Miglio 2013).

Interestingly, GSC 09289–02186 and GSC 04281–00186 exhibit the highest principal pulsation frequencies of all our sample stars (2.33692 d^{-1} and 2.16673 d^{-1}, respectively). Further detailed studies

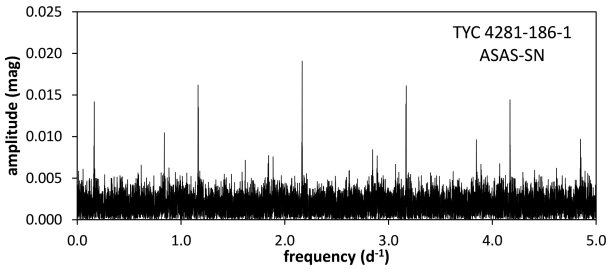

Figure 8. Fourier amplitude spectrum of the G-type giant pulsator GSC 04281–00186, based on unwhitened ASAS-SN data. The *y*-axis denotes semi-amplitudes, as derived with PERIOD04.

of these objects are encouraged, which might shed light on their pulsational properties and the mechanisms at work and could, perhaps, lead to another expansion of the class defintion of GDOR stars. This, however, is out of the scope of the present investigation.

5 CONCLUSION

We have investigated high-amplitude GDOR (HAGDOR) stars showing light variability amplitudes well beyond the traditional 0.1 mag (V) limit, with the aim of unraveling the mechanisms behind the observed high amplitudes and investigating whether these objects are in any way physically distinct from regular GDOR stars ($V_{\rm amp} \leq 0.1$ mag). To this end, a sample of 15 HAGDOR stars and a control sample of 20 regular GDOR stars boasting extensive photometric time series data were collected.

As a first step, we calculated astrophysical parameters and investigated our sample stars in the $\log T_{\rm eff}$ versus $\log L/L_{\odot}$ diagram. No

significant differences between the location of the HAGDOR stars and the GDOR stars were found – both groups are well distributed over the whole main sequence up to $\log L/L_{\odot} < 1.1$. Employing publicly available survey data (*Kepler*, ASAS-3, ASAS-SN, and, in the case of one star, *TESS* data) and our own observations, we analysed the photometric variability of our target stars, using the well-described HAGDOR star KIC 8113425 (Kurtz et al. 2015) as a model case.

We found that all HAGDOR variables show light curves of the ASYM type and behave similarly to KIC 8113425 in that they exhibit multiple frequencies whose beating results in total amplitudes considerably exceeding the amplitudes of the base frequencies. Hence, the high amplitudes observed in the HAGDOR stars can be explained by the superposition of several base frequencies in interaction with their combination and overtone frequencies. Although the maximum amplitude of the primary frequencies does not exceed an amplitude of 0.1 mag, total light variability amplitudes of over 0.3 mag (V) can be attained in this way – important input for pulsational modelling attempts. We conclude that a revision of the traditional amplitude cut-off of 0.1 mag (V) for GDOR stars is necessary. Based on the analyses of the present investigation, we propose a new cut-off value of 0.35 mag (V). We caution, however, that this conclusion has been based on the analysis of a small sample and HAGDOR stars with larger amplitudes may be found subsequently.

To tackle the question whether HAGDOR stars and GDOR stars are physically distinct objects, correlations between the observed primary frequencies, amplitudes, and other parameters like effective temperature and luminosity were investigated. HAGDOR stars tend to show larger amplitudes, and nearly all of the investigated stars exhibit closely spaced primary frequencies, which seems to be a general characteristic of the class of GDOR variables. Apart from that, however, no significant differences were found; instead, both groups overlap and show gradual transitions in the investigated parameter spaces. We therefore conclude that low- and high-amplitude GDOR stars are not physically distinct in any other respect than their total variability amplitudes but merely represent two ends of the same, uniform group of variables. However, we caution that the sample sizes used for our investigation are small (15 HAGDOR stars and a comparison sample of 20 regular GDOR stars with total variability amplitudes of $0.05 \leq V \leq 0.1$ mag); our conclusions, therefore, should be confirmed using a larger sample of stars with good photometric time series observations.

We call attention to the GDOR variables GSC 09289–02186 and GSC 04281–00186, which exhibit the highest principal pulsation frequencies of our sample stars. Furthermore, both stars are situated outside the traditional boundaries of the GDOR realm and constitute the most obvious outliers in the investigated parameter spaces. Although some discrepancies in the available data exist, according to its calibrated astrophysical parameters, GSC 04281–00186 is a G-type giant, which is intriguing as GDOR stars belong to luminosity classes IV or V by definition. Further detailed studies of these objects are encouraged.

ACKNOWLEDGEMENTS

We thank the referee for *his/her* thoughtful report that helped to improve this paper. This research has made use of the SIMBAD and VizieR databases operated at the Centre de Données Astronomiques (Strasbourg) in France, of the AAVSO International Variable Star Index (VSX) and of the Two Micron All Sky Survey (2MASS), which is a joint project of the University of Massachusetts and the Infrared Processing and Analysis Center/California Institute of Technology, funded by the National Aeronautics and Space Administration and the National Science Foundation. This paper includes data collected by the *Kepler* mission. Funding for the *Kepler* mission is provided by the NASA Science Mission directorate. This paper includes data collected with the *TESS* mission, obtained from the MAST data archive at the Space Telescope Science Institute (STScI). Funding for the *TESS* mission is provided by the NASA Explorer Program. STScI is operated by the Association of Universities for Research in Astronomy, Inc., under NASA contract NAS 5-26555. This work has also made use of data from the European Space Agency (ESA) mission *Gaia* (http://www.cosmos.esa.int/gaia), processed by the Gaia Data Processing and Analysis Consortium (DPAC, http://www.cosmos.esa.int/web/gaia/dpac/consortium). Funding for the DPAC has been provided by national institutions, in particular the institutions participating in the Gaia Multilateral Agreement. Guoshoujing Telescope (the Large Sky Area Multi-Object Fiber Spectroscopic Telescope LAMOST) is a National Major Scientific Project built by the Chinese Academy of Sciences. Funding for the project has been provided by the National Development and Reform Commission. LAMOST is operated and managed by the National Astronomical Observatories, Chinese Academy of Sciences.

DATA AVAILABILITY

The data underlying this article will be shared on reasonable request to the corresponding author.

REFERENCES

Ammons S. M., Robinson S. E., Strader J., Laughlin G., Fischer D., Wolf A., 2006, ApJ, 638, 1004
Antoci V. et al., 2019, MNRAS, 490, 4040
Arenou F. et al., 2018, A&A, 616, A17
Balona L. A., 2012, in Shibahashi H., Takata M., Lynas-Gray A. E., eds, ASP Conf. Ser. Vol. 462, Progress in Solar/Stellar Physics with Helio- and Asteroseismology. Astron. Soc. Pac., San Francisco, p. 118
Balona L. A., 2018, Frontiers Astron. Space Sci., 5, 43
Balona L. A., Krisciunas K., Cousins A. W. J., 1994, MNRAS, 270, 905
Balona L. A., Guzik J. A., Uytterhoeven K., Smith J. C., Tenenbaum P., Twicken J. D., 2011, MNRAS, 415, 3531
Balona L. A. et al., 2016, MNRAS, 460, 1318
Bedding T. R. et al., 2010, ApJ, 713, L176
Borucki W. J. et al., 2010, Science, 327, 977
Bourgés L., Lafrasse S., Mella G., Chesneau O., Bouquin J. L., Duvert G., Chelli A., Delfosse X., 2014, in Manset N., Forshay P., eds, ASP Conf. Ser. Vol. 485, Astronomical Data Analysis Software and Systems XXIII. Astron. Soc. Pac., San Francisco, p. 223
Bradley P. A., Guzik J. A., Miles L. F., Uytterhoeven K., Jackiewicz J., Kinemuchi K., 2015, AJ, 149, 68
Breger M., 2000, in Breger M., Montgomery M., eds, ASP Conf. Ser. Vol. 210, Delta Scuti and Related Stars. Astron. Soc. Pac., San Francisco, p. 3
Breger M., Pamyatnykh A. A., 1998, A&A, 332, 958
Breger M. et al., 1993, A&A, 271, 482
Brown T. M., Latham D. W., Everett M. E., Esquerdo G. A., 2011, AJ, 142, 112
Campante T. L. et al., 2016, ApJ, 830, 138
Chaplin W. J., Miglio A., 2013, ARA&A, 51, 353
Claret A., 1995, A&AS, 109, 441
Cui X.-Q. et al., 2012, Res. Astron. Astrophys., 12, 1197
David M., Hensberge H., Nitschelm C., 2014, J. Astron. Data, 20, 1
De Cat P. et al., 2015, ApJS, 220, 19
Dupret M.-A., Grigahcène A., Garrido R., Gabriel M., Scuflaire R., 2004, A&A, 414, L17
Dupret M. A., Grigahcène A., Garrido R., Gabriel M., Scuflaire R., 2005, A&A, 435, 927

Fath E. A., 1935, Lick Obs. Bull., 17, 175
Frasca A. et al., 2016, A&A, 594, A39
Gaia Collaboration et al., 2016, A&A, 595, A1
Gaia Collaboration et al., 2018, A&A, 616, A1
Gilliland R. L. et al., 2010, PASP, 122, 131
Gray R. O. et al., 2016, AJ, 151, 13
Green G. M. et al., 2018, MNRAS, 478, 651
Grigahcène A. et al., 2010, ApJ, 713, L192
Guzik J. A., Kaye A. B., Bradley P. A., Cox A. N., Neuforge C., 2000, ApJ, 542, L57
Hambsch F.-J., 2012, J. Am. Assoc. Var. Star Obs., 40, 1003
Handler G., Shobbrook R. R., 2002, MNRAS, 333, 251
Henden A. A., Levine S., Terrell D., Welch D., 2015, APASS - The Latest Data Release, American Astronomical Society Meeting Abstracts, Vol. 225, p. 336.16
Henry G. W., Fekel F. C., 2005, AJ, 129, 2026
Houk N., 1982, Michigan Catalogue of Two-dimensional Spectral Types for the HD stars, Univ. Michigan, Ann Harbor, MI
Houk N., Cowley A. P., 1975, University of Michigan Catalogue of two-dimensional spectral types for the HD stars, Univ. Michigan, Ann Harbor, MI
Houk N., Smith-Moore M., 1988, Michigan Catalogue of Two-dimensional Spectral Types for the HD Stars, Univ. Michigan, Ann Harbor, MI
Huber D. et al., 2014, ApJS, 211, 2
Jayasinghe T. et al., 2018, MNRAS, 477, 3145
Johnson H. L., Morgan W. W., 1951, ApJ, 114, 522
Kahraman Aliçavuş F., Poretti E., Catanzaro G., Smalley B., Niemczura E., Rainer M., Handler G., 2020, MNRAS, 493, 4518
Kaye A. B., Handler G., Krisciunas K., Poretti E., Zerbi F. M., 1999, PASP, 111, 840
Kharchenko N. V., 2001, Kinematika Fizika Nebesnykh Tel, 17, 409
Koch D. G. et al., 2010, ApJ, 713, L79
Kochanek C. S. et al., 2017, PASP, 129, 104502
Kunder A. et al., 2017, AJ, 153, 75
Kurtz D. W., Shibahashi H., Murphy S. J., Bedding T. R., Bowman D. M., 2015, MNRAS, 450, 3015
Lenz P., Breger M., 2005, Commun. Asteroseismology, 146, 53
McDonald I., Zijlstra A. A., Boyer M. L., 2012, MNRAS, 427, 343
McNamara D. H., 2000, in Breger M., Montgomery M., eds, ASP Conf. Ser. Vol. 210, Delta Scuti and Related Stars. Astron. Soc. Pac., San Francisco, p. 373
Munari U. et al., 2014, AJ, 148, 81
Ochsenbein F., 1980, Bull. Inf. Cent. Donnees Stellaires, 19, 74
Paunzen E., Netopil M., Herdin A., 2017, Bulgarian Astron. J., 26, 45
Pecaut M. J., Mamajek E. E., 2013, ApJS, 208, 9
Pigulski A., 2014, in Guzik J. A., Chaplin W. J., Handler G., Pigulski A., eds, Proc. IAU Symp. 301, Precision Asteroseismology. Kluwer, Dordrecht, p. 31
Pinsonneault M. H., An D., Molenda-Żakowicz J., Chaplin W. J., Metcalfe T. S., Bruntt H., 2012, ApJS, 199, 30
Pojmański G., 2002, AcA, 52, 397
Ricker G. R. et al., 2014, SPIE Journal of Astronomical Telescopes, Instruments, and Systems (JATIS), Vol. 9143, p. 914320
Ricker G. R. et al., 2015, J. Astron. Telescopes, Instrum., Syst., 1, 014003
Samus N. N., Kazarovets E.V., Durlevich O.V., Kireeva N.N., Pastukhova E.N., 2017, Astronomy Reports, 61, 80
Shappee B. J. et al., 2014, ApJ, 788, 48
Skiff B. A., 2014, Catalogue of Stellar Spectral Classifications, VizieR Online Data Catalog: B/mk, 1
Straižys V., Lazauskaitė R., 2009, Baltic Astron., 18, 19
Tkachenko A., Lehmann H., Smalley B., Debosscher J., Aerts C., 2012, MNRAS, 422, 2960
Uytterhoeven K. et al., 2011, A&A, 534, A125
Watson C. L., 2006, Soc. Astron. Sci. Annu. Symp., 25, 47
Wright C. O., Egan M. P., Kraemer K. E., Price S. D., 2003, AJ, 125, 359
Zhao G., Zhao Y.-H., Chu Y.-Q., Jing Y.-P., Deng L.-C., 2012, Res. Astron. Astrophys., 12, 723

APPENDIX A: FREQUENCY SOLUTIONS

In the following, the frequency solutions for all sample stars are presented in tabular form. Stars are listed in order of increasing right ascension. In each table, the columns denote: (1) frequency number; (2) frequency value; (3) semi-amplitude; (4) corresponding phase; and (5) frequency identification. All values were derived using PERIOD04, as outlined in Section 3.6.

Table A1. Frequency solution for *GSC 02831–00348* (V0758 And).

(1) Frequency number	(2) Frequency	(3) Amplitude	(4) Phase	(5) ID
$F1_{\text{ASAS-SN}}$	1.081484	0.052	0.6574	f_1
$F2_{\text{ASAS-SN}}$	1.155404	0.010	0.7579	f_2

Table A2. Frequency solution for *HD 17721* (HIP 13089).

(1) Frequency number	(2) Frequency	(3) Amplitude	(4) Phase	(5) ID
$F1_{\text{ASAS-3}}$	0.919238	0.025	0.3389	f_1
$F2_{\text{ASAS-3}}$	0.774241	0.007	0.2701	f_2
$F1_{\text{TESS}}$	0.919038	0.0192	0.2682	f_1
$F2_{\text{TESS}}$	0.776222	0.0090	0.9202	f_2
$F3_{\text{TESS}}$	0.653821	0.0057	0.8019	f_3
$F4_{\text{TESS}}$	1.120093	0.0056	0.5962	f_4
$F5_{\text{TESS}}$	0.196703	0.0045	0.5247	f_5

Table A3. Frequency solution for *HD 33575* (NSV 1858).

(1) Frequency number	(2) Frequency	(3) Amplitude	(4) Phase	(5) ID
$F1_{\text{ASAS-3}}$	0.773239	0.032	0.3632	f_1
$F2_{\text{ASAS-3}}$	0.652773	0.025	0.9155	f_2
$F3_{\text{ASAS-3}}$	1.425986	0.024	0.6162	$f_1 + f_2$
$F1_{\text{ASAS-SN}}$	0.773220	0.044	0.6462	f_1
$F2_{\text{ASAS-SN}}$	0.652721	0.033	0.1973	f_2

Table A4. Frequency solution for *HD 50875* (NSV 3272).

(1) Frequency number	(2) Frequency	(3) Amplitude	(4) Phase	(5) ID
$F1_{\text{ASAS-3}}$	0.586397	0.026	0.2689	f_1
$F2_{\text{ASAS-3}}$	0.692966	0.021	0.5241	f_2
$F3_{\text{ASAS-3}}$	0.110471	0.011	0.9279	$f_2 - f_1$?

Table A5. Frequency solution for *HD 85693* (NSV 18291).

(1) Frequency number	(2) Frequency	(3) Amplitude	(4) Phase	(5) ID
$F1_{\text{ASAS-3}}$	0.888140	0.034	0.8495	f_1
$F2_{\text{ASAS-3}}$	0.778475	0.021	0.9916	f_2
$F3_{\text{ASAS-3}}$	1.666578	0.014	0.2639	$f_1 + f2$
$F4_{\text{ASAS-3}}$	0.793137	0.012	0.0540	f_3

Table A6. Frequency solution for *GSC 09046–00646* (ASAS J163451-6446.3).

(1) Frequency number	(2) Frequency	(3) Amplitude	(4) Phase	(5) ID
$F1_{\text{ASAS-3}}$	0.846993	0.025	0.9727	f_1
$F2_{\text{ASAS-3}}$	0.560801	0.020	0.1025	f_2
$F1_{\text{ASAS-SN}}$	0.560868	0.023	0.3169	f_2
$F2_{\text{ASAS-SN}}$	0.847028	0.024	0.0205	f_1

Table A7. Frequency solution for *HD 150538* (NSV 20738).

(1) Frequency number	(2) Frequency	(3) Amplitude	(4) Phase	(5) ID
$F1_{\text{ASAS-3}}$	0.721031	0.033	0.4240	f_1
$F2_{\text{ASAS-3}}$	1.140350	0.020	0.9765	f_2
$F3_{\text{ASAS-3}}$	1.044124	0.013	0.0028	f_3

Table A8. Frequency solution for *KIC 3847822* (TYC 3134-2121-1).

(1) Frequency number	(2) Frequency	(3) Amplitude	(4) Phase	(5) ID
$F1_{\text{ASAS-SN}}$	0.829894	0.018	0.5224	f_1
$F2_{\text{ASAS-SN}}$	0.963088	0.017	0.3484	f_2
$F3_{\text{ASAS-SN}}$	0.915570	0.011	0.0795	f_2
$F1_{\text{Kepler}}$	0.829875	0.01600	0.6923	f_1
$F2_{\text{Kepler}}$	0.963154	0.01494	0.7443	f_2
$F3_{\text{Kepler}}$	0.915471	0.00771	0.8871	f_3
$F4_{\text{Kepler}}$	1.096999	0.00762	0.9753	f_4
$F5_{\text{Kepler}}$	0.133330	0.00673	0.5757	$f_2 - f_1$
$F6_{\text{Kepler}}$	0.085594	0.00347	0.0515	$f_3 - f_1$
$F7_{\text{Kepler}}$	0.047627	0.00345	0.1426	$f_2 - f_3$
$F8_{\text{Kepler}}$	0.267117	0.00339	0.1179	$f_4 - f_1$
$F9_{\text{Kepler}}$	0.133790	0.00420	0.3820	$f_4 - f_2$
$F10_{\text{Kepler}}$	0.781546	0.00277	0.0652	f_5
$F11_{\text{Kepler}}$	0.181559	0.00259	0.7470	$f_4 - f_3$

Table A9. Frequency solution for *KIC 3441414* (GSC 03134–00901).

(1) Frequency number	(2) Frequency	(3) Amplitude	(4) Phase	(5) ID
$F1_{\text{ASAS-SN}}$	1.233502	0.021	0.5729	f_1
$F2_{\text{ASAS-SN}}$	1.107843	0.010	0.7617	f_2
$F3_{\text{ASAS-SN}}$	1.321001	0.007	0.2928	f_3
$F1_{\text{Kepler}}$	1.233479	0.01841	0.1633	f_1
$F2_{\text{Kepler}}$	1.107875	0.01237	0.8904	f_2
$F3_{\text{Kepler}}$	1.320999	0.00622	0.6805	f_3
$F4_{\text{Kepler}}$	0.125600	0.00350	0.1636	$f_1 - f_2$
$F5_{\text{Kepler}}$	2.341354	0.00230	0.3444	$f_1 + f_2$
$F6_{\text{Kepler}}$	0.543345	0.00176	0.3657	f_4
$F7_{\text{Kepler}}$	0.962388	0.00170	0.4148	f_5
$F8_{\text{Kepler}}$	2.466959	0.00164	0.6123	$2f_1$
$F9_{\text{Kepler}}$	1.465986	0.00138	0.7528	f_6
$F10_{\text{Kepler}}$	0.087513	0.00134	0.4919	$f_3 - f_1$
$F11_{\text{Kepler}}$	1.179790	0.00130	0.4088	f_7

Table A9 – *continued*

(1) Frequency number	(2) Frequency	(3) Amplitude	(4) Phase	(5) ID
$F12_{\text{Kepler}}$	0.213140	0.00120	0.6362	$f_3 - f_2$
$F13_{\text{Kepler}}$	0.508685	0.00109	0.6989	f_8
$F14_{\text{Kepler}}$	1.661927	0.00109	0.3922	f_9
$F15_{\text{Kepler}}$	1.742302	0.00108	0.0020	f_{10}
$F16_{\text{Kepler}}$	1.359081	0.00105	0.6474	$2f_1 - f_2$
$F17_{\text{Kepler}}$	0.034023	0.00102	0.4082	$-2f_1 + f_3 + f_7$
$F18_{\text{Kepler}}$	1.652501	0.00095	0.9946	$f_1 - f_4 + f_5$

Table A10. Frequency solution for *KIC 7448050* (ASAS J193103+4302.1).

(1) Frequency number	(2) Frequency	(3) Amplitude	(4) Phase	(5) ID
$F1_{\text{ASAS-SN}}$	1.139451	0.031	0.9378	f_1
$F2_{\text{ASAS-SN}}$	1.043578	0.014	0.3619	f_2
$F3_{\text{ASAS-SN}}$	1.560555	0.013	0.7565	f_3
$F4_{\text{ASAS-SN}}$	2.278806	0.006	0.8760	$2f_1$
$F1_{\text{Kepler}}$	1.139452	0.02766	0.9283	f_1
$F2_{\text{Kepler}}$	1.043526	0.01312	0.7471	f_2
$F3_{\text{Kepler}}$	1.560513	0.00949	0.0753	f_3
$F4_{\text{Kepler}}$	1.282439	0.00790	0.7678	f_4
$F5_{\text{Kepler}}$	0.421057	0.00404	0.0003	$f_3 - f_1$
$F6_{\text{Kepler}}$	1.785288	0.00347	0.2634	f_5
$F7_{\text{Kepler}}$	0.237194	0.00311	0.8573	$f_4 - f_2$
$F8_{\text{Kepler}}$	2.182984	0.00298	0.9297	$f_1 + f_2$
$F9_{\text{Kepler}}$	1.376648	0.00297	0.0357	f_6
$F10_{\text{Kepler}}$	1.399469	0.00279	0.0933	f_7
$F11_{\text{Kepler}}$	0.142968	0.00277	0.8800	$f_4 - f_1$

Table A11. Frequency solution for *KIC 6953103* (2MASS J19325124+4228465).

(1) Frequency number	(2) Frequency	(3) Amplitude	(4) Phase	(5) ID
$F1_{\text{Kepler}}$	1.287599	0.03357	0.7980	f_1
$F2_{\text{Kepler}}$	1.115789	0.02269	0.5773	f_2
$F3_{\text{Kepler}}$	1.198750	0.02199	0.1149	f_3
$F4_{\text{Kepler}}$	0.171818	0.00959	0.0547	$f_1 - f_2$
$F5_{\text{Kepler}}$	0.088856	0.00802	0.6031	$f_1 - f_3$
$F6_{\text{Kepler}}$	1.026945	0.00601	0.7031	$f_2 + f_3 - f_1$
$F7_{\text{Kepler}}$	2.403390	0.00534	0.6671	$f_1 + f_2$
$F8_{\text{Kepler}}$	1.254955	0.00517	0.4008	f_4
$F9_{\text{Kepler}}$	0.071200	0.00505	0.3261	$f_5 - f_1$
$F10_{\text{Kepler}}$	1.358803	0.00461	0.3727	f_5
$F11_{\text{Kepler}}$	2.486359	0.00467	0.1549	$f_1 + f_3$
$F12_{\text{Kepler}}$	1.376442	0.00452	0.7867	$2f_1 - f_3$
$F13_{\text{Kepler}}$	2.575187	0.00428	0.9824	$2f_1$
$F14_{\text{Kepler}}$	2.314550	0.00386	0.8803	$f_2 + f_3$
$F15_{\text{Kepler}}$	1.186985	0.00374	0.1643	$-f_1 + f_2 + f_5$
$F16_{\text{Kepler}}$	1.459425	0.00344	0.1386	$2f_1 - f_2$
$F17_{\text{Kepler}}$	0.082985	0.00338	0.2898	$-f_2 + f_3$
$F18_{\text{Kepler}}$	0.943990	0.00319	0.8789	$-f_1 + 2f_2$
$F19_{\text{Kepler}}$	2.474589	0.00306	0.2586	$f_2 + f_5$
$F20_{\text{Kepler}}$	1.132902	0.00305	0.4786	f_6

Table A12. Frequency solution for *KIC 8113425* (2MASS J19474808+4354257).

(1) Frequency number	(2) Frequency	(3) Amplitude	(4) Phase	(5) ID
$F1_{\mathrm{ASAS\text{-}SN}}$	0.429956	0.014	0.7265	f_1
$F2_{\mathrm{ASAS\text{-}SN}}$	0.489422	0.011	0.2704	f_2
$F3_{\mathrm{ASAS\text{-}SN}}$	0.449965	0.008	0.2736	f_3
$F1_{\mathrm{Kepler}}$	0.430055	0.01428	0.5268	f_1
$F2_{\mathrm{Kepler}}$	0.489411	0.01285	0.9223	f_2
$F3_{\mathrm{Kepler}}$	0.450101	0.00990	0.1920	f_3
$F4_{\mathrm{Kepler}}$	0.461260	0.00763	0.4039	f_4
$F5_{\mathrm{Kepler}}$	0.919451	0.00706	0.7664	f_1+f_2
$F6_{\mathrm{Kepler}}$	0.950674	0.00636	0.4393	f_2+f_4
$F7_{\mathrm{Kepler}}$	0.891334	0.00483	0.9490	f_1+f_4
$F8_{\mathrm{Kepler}}$	0.059311	0.00445	0.6557	f_2-f_1
$F9_{\mathrm{Kepler}}$	0.978781	0.00418	0.3443	$2f_2$
$F10_{\mathrm{Kepler}}$	0.008106	0.00352	0.8156	$f_1+f_2-f_3-f_4$
$F11_{\mathrm{Kepler}}$	0.398841	0.00363	0.3539	$2f_1-f_4$
$F12_{\mathrm{Kepler}}$	1.380730	0.00328	0.2701	$f_1+f_2+f_4$

Table A13. Frequency solution for *KIC 7304385* (ASAS J195052+4248.1).

(1) Frequency number	(2) Frequency	(3) Amplitude	(4) Phase	(5) ID
$F1_{\mathrm{Kepler}}$	1.269238	0.02562	0.9781	f_1
$F2_{\mathrm{Kepler}}$	1.418047	0.02075	0.1262	f_2
$F3_{\mathrm{Kepler}}$	1.462331	0.00796	0.6361	f_3
$F4_{\mathrm{Kepler}}$	0.148812	0.00671	0.0651	f_2-f_1
$F5_{\mathrm{Kepler}}$	1.487632	0.00467	0.1299	f_4
$F6_{\mathrm{Kepler}}$	2.687285	0.00408	0.4037	f_2+f_1
$F7_{\mathrm{Kepler}}$	1.120411	0.00296	0.9132	$2f_1-f_2$
$F8_{\mathrm{Kepler}}$	1.243951	0.00301	0.9347	$f_1+f_3-f_4$
$F9_{\mathrm{Kepler}}$	2.538475	0.00294	0.2640	$2f_1$
$F10_{\mathrm{Kepler}}$	0.635646	0.00242	0.1740	f_5
$F11_{\mathrm{Kepler}}$	0.193106	0.00242	0.5330	$-f_1+f_3$
$F12_{\mathrm{Kepler}}$	1.566863	0.00229	0.4698	$2f_2-f_1$
$F13_{\mathrm{Kepler}}$	1.076156	0.00234	0.8462	$2f_1-f_3$
$F14_{\mathrm{Kepler}}$	1.180661	0.00211	0.3085	$f_1-2f_3+2f_2$
$F15_{\mathrm{Kepler}}$	0.152996	0.00184	0.8403	$-2f_1+f_2+2f_5$
$F16_{\mathrm{Kepler}}$	2.053669	0.00175	0.5396	f_2+f_5
$F17_{\mathrm{Kepler}}$	1.116238	0.00167	0.9054	f_6
$F18_{\mathrm{Kepler}}$	1.095130	0.00166	0.9118	$2f_1+f_3-f_2-f_4$
$F19_{\mathrm{Kepler}}$	1.031884	0.00152	0.2022	$2f_1+f_2-2f_3$
$F20_{\mathrm{Kepler}}$	1.378640	0.00152	0.8504	$f_1+2f_6-f_4-f_5$
$F21_{\mathrm{Kepler}}$	2.836090	0.00150	0.6154	$2f_2$

Table A14. Frequency solution for *HD 211394* (BD–17 6481).

(1) Frequency number	(2) Frequency	(3) Amplitude	(4) Phase	(5) ID
$F1_{\mathrm{ASAS\text{-}3}}$	0.452407	0.049	0.7275	f_1
$F2_{\mathrm{ASAS\text{-}3}}$	0.371387	0.027	0.6153	f_2
$F3_{\mathrm{ASAS\text{-}3}}$	0.904804	0.020	0.7111	$2f_1$
$F4_{\mathrm{ASAS\text{-}3}}$	0.823776	0.018	0.6548	f_1+f_2
$F5_{\mathrm{ASAS\text{-}3}}$	1.276179	0.014	0.6848	f_2+2f_1
$F1_{\mathrm{ROAD}}$	0.452625	0.051	0.0744	f_1
$F2_{\mathrm{ROAD}}$	0.370860	0.026	0.7140	f_2
$F3_{\mathrm{ROAD}}$	0.823041	0.020	0.4374	f_1+f_2
$F4_{\mathrm{ROAD}}$	0.904372	0.018	0.1150	$2f_1$
$F1_{\mathrm{Kepler}}$	0.452538	0.04193	0.8082	f_1
$F2_{\mathrm{Kepler}}$	0.372089	0.01975	0.7546	f_2
$F3_{\mathrm{Kepler}}$	0.905160	0.01774	0.2723	$2f_1$
$F4_{\mathrm{Kepler}}$	0.824686	0.01274	0.4111	f_1+f_2
$F5_{\mathrm{Kepler}}$	0.080533	0.01063	0.3164	f_1-f_2
$F6_{\mathrm{Kepler}}$	1.005225	0.01002	0.3856	f_3
$F7_{\mathrm{Kepler}}$	0.533652	0.00904	0.2196	$2f_1-f_2$
$F8_{\mathrm{Kepler}}$	1.357718	0.00816	0.2133	f_4

Table A15. Frequency solution for *GSC 02780-02174* (TYC 2780-2174-1).

(1) Frequency number	(2) Frequency	(3) Amplitude	(4) Phase	(5) ID
$F1_{\mathrm{ASAS\text{-}SN}}$	1.059750	0.034	0.3190	f_1
$F2_{\mathrm{ASAS\text{-}SN}}$	1.245288	0.013	0.8264	f_2
$F3_{\mathrm{ASAS\text{-}SN}}$	1.476331	0.008	0.9466	f_3
$F4_{\mathrm{ASAS\text{-}SN}}$	1.114903	0.008	0.4843	f_4

APPENDIX B: FOURIER AMPLITUDE SPECTRA

This section provides the Fourier amplitude spectra of all HAGDOR stars, based on unwhitened data. The *y*-axes denote semi-amplitudes, as derived with PERIOD04. The employed data source is indicated in the panels. More information on the period analysis is provided in Section 3.6.

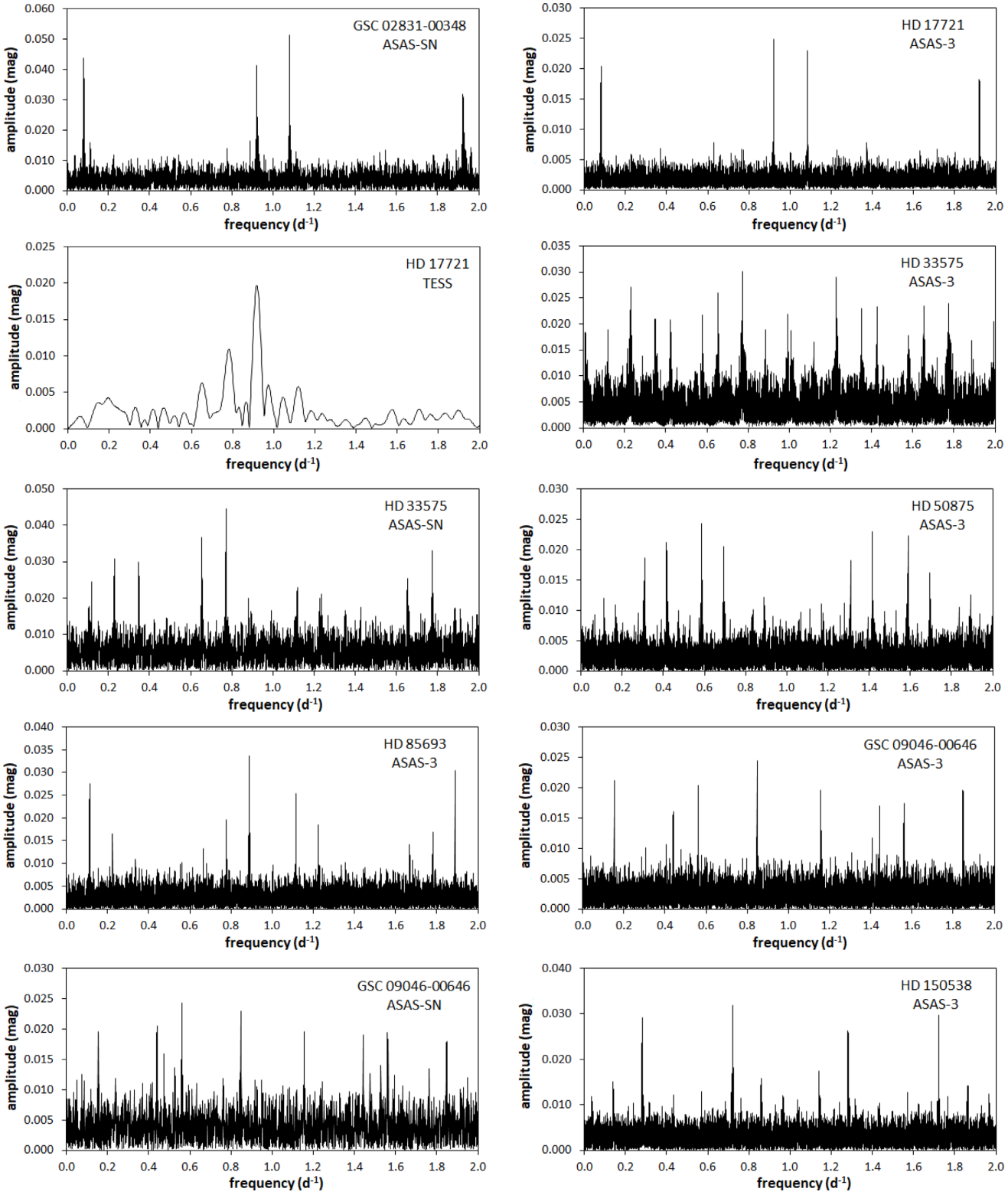

Figure B1. Fourier amplitude spectra for all HAGDOR stars, based on unwhitened data. The employed data source is indicated in the panels.

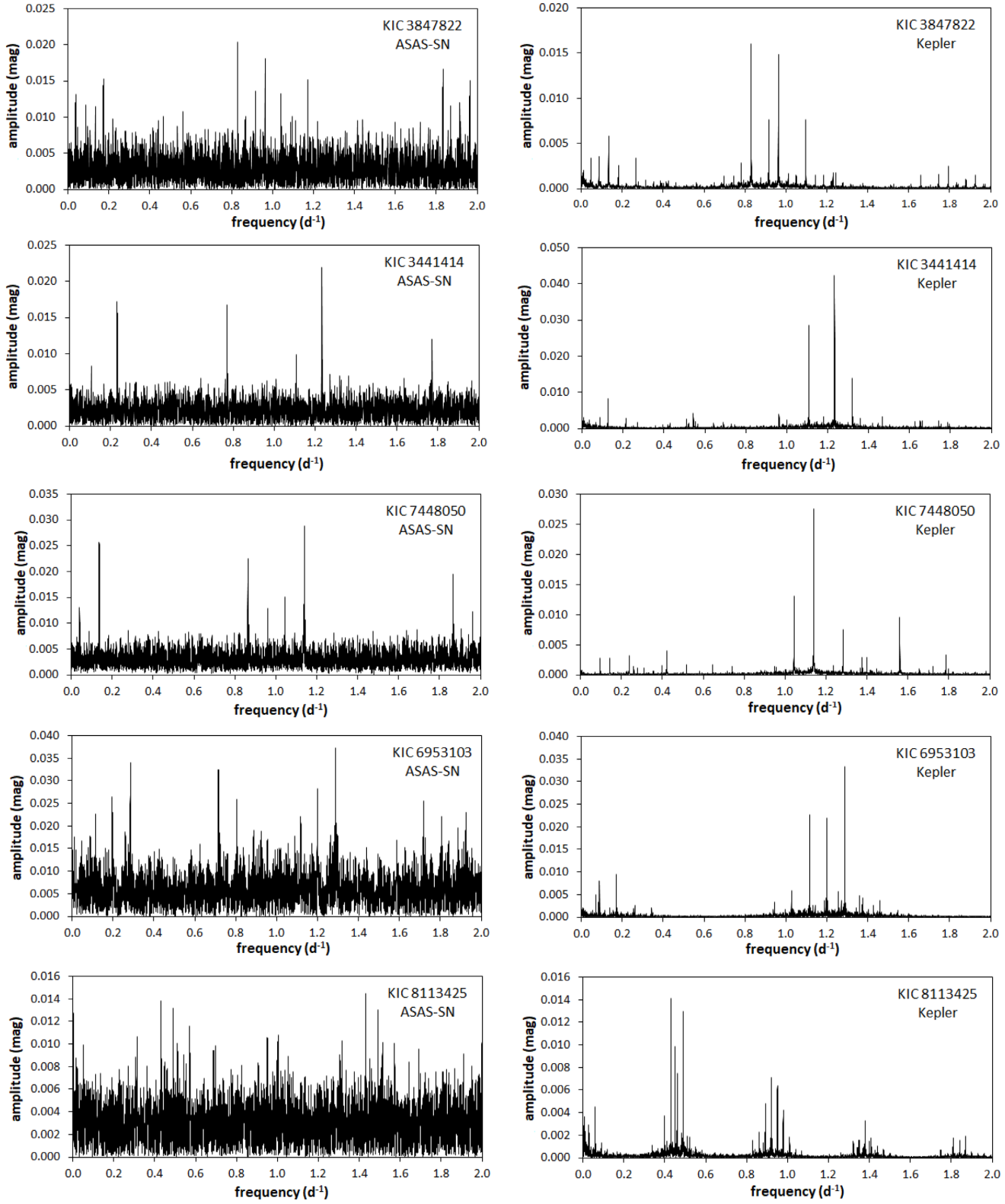

Figure B1 – *continued*

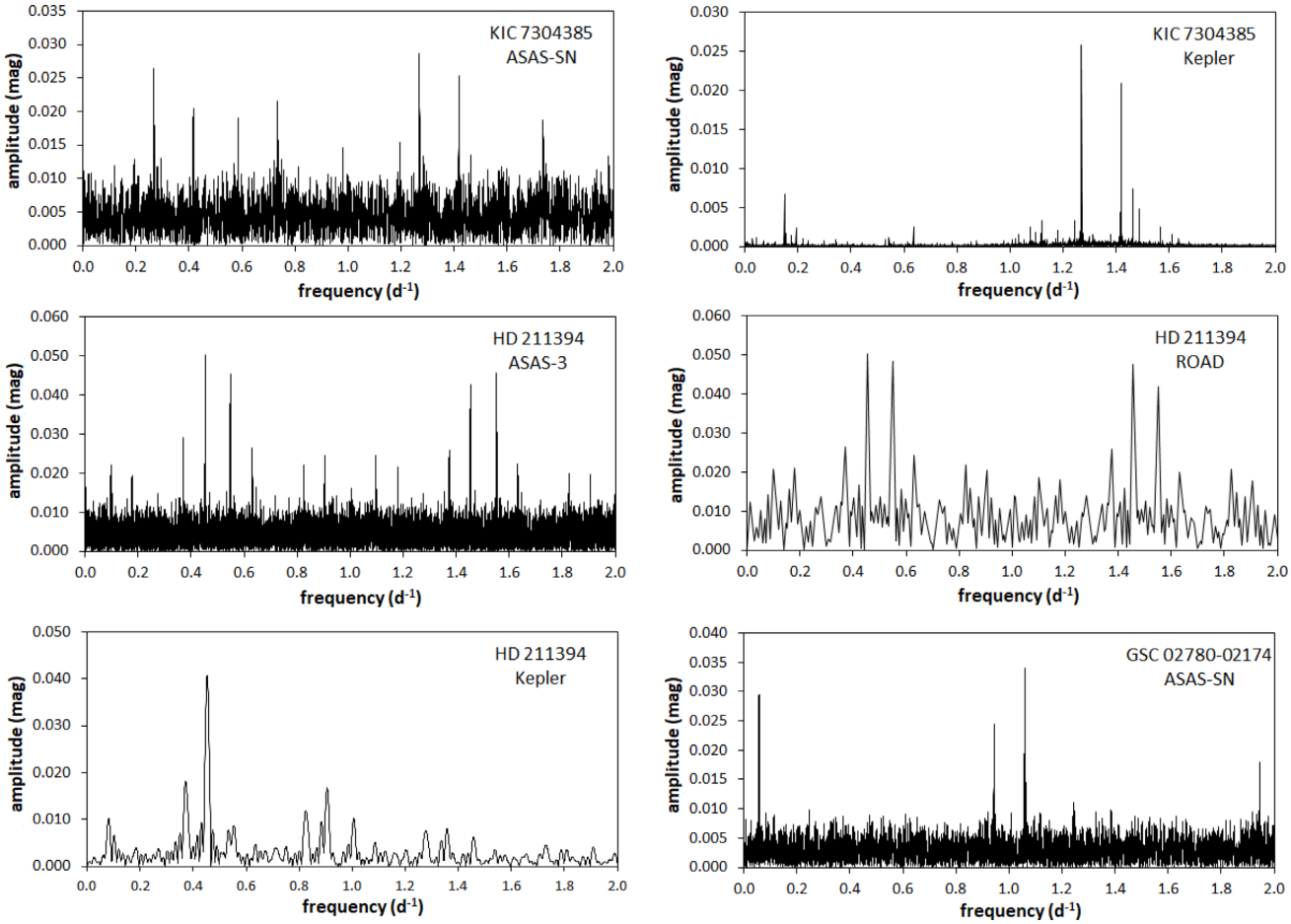

Figure B1 – *continued*

This paper has been typeset from a TEX/LATEX file prepared by the author.